



An investigation of silver electrodeposition from ionic liquids: Influence of atmospheric water uptake on the silver electrodeposition mechanism and film morphology

Andrew Basile^{a,b}, Anand I. Bhatt^{b,*}, Anthony P. O'Mullane^{a,**,1}, Suresh K. Bhargava^a

^a School of Applied Sciences, RMIT University, G.P.O. Box 2476V, Melbourne, Victoria 3001, Australia

^b CSIRO Energy Technology, Clayton, Victoria 3169, Australia

ARTICLE INFO

Article history:

Received 9 December 2010

Accepted 29 December 2010

Available online 8 January 2011

Keywords:

Ionic liquid

Silver electrodeposition

Nucleation–growth

ABSTRACT

The electrodeposition of silver from two ionic liquids, 1-butyl-3-methylimidazolium tetrafluoroborate ([BMIm][BF₄]) and N-butyl-N-methyl-pyrrolidinium bis(trifluoromethanesulfonyl)imide ([C₄mPyr][TFSI]), and an aqueous KNO₃ solution on a glassy carbon electrode was undertaken. It was found by cyclic voltammetry that the electrodeposition of silver proceeds through nucleation–growth kinetics. Analysis of chronoamperometric data indicated that the nucleation–growth mechanism is instantaneous at all potentials in the case of [BMIm][BF₄] and [C₄mPyr][TFSI], and instantaneous at low overpotentials tending to progressive at high overpotentials for KNO₃. Significantly, under ambient conditions, the silver electrodeposition mechanism changes to progressive nucleation and growth in [C₄mPyr][TFSI], which is attributed to the uptake of atmospheric water in the IL. It was found that these differences in the growth mechanism impact significantly on the morphology of the resultant electrodeposit which is characterised *ex situ* by scanning electron microscopy and X-ray diffraction.

© 2011 Elsevier Ltd. All rights reserved.

1. Introduction

The electrodeposition of metals from ionic liquids (ILs) has received significant interest. A recent review of this topic demonstrated that a host of metals and alloys can be deposited in ionic liquids due to their inherent properties such as chemical stability, low/negligible vapour pressures, high ionic conductivity and wide electrochemical window [1,2]. Compared to the currently used solvents, the use of ionic liquids offers distinct advantages, such as operating open plating baths at variable temperatures without the release of harmful vapours and a lack of any hydrogen embrittlement processes due to the hydrophobic nature of many ionic liquids [3,4].

There are many industrial applications that require homogeneous metal thin films. In particular, the electrodeposition of silver is an important process given its use in microelectronics, jewellery, aerospace and anti-bacterial applications [3,5,6]. Several approaches have been taken to produce silver films including physical vapour deposition, chemical vapour deposition and sputtering,

all of which have disadvantages including cost and slow deposition rates. Other approaches include electro and electroless plating, however, this usually requires the use of toxic cyanide based plating baths that often contain additional organic additives, which are both harmful and difficult to dispose of after the reaction completes. Therefore, the development of alternative solvents that minimise the use of pollutants is of importance given the industrial and academic focus on green processes which aim to reduce the environmental impact of current industrial methods.

The electrodeposition of silver from ionic liquids has been suggested as an alternative to aqueous based electroplating baths. Initial electrodeposition studies focussed on the use of chloroaluminate melts [7–10], however, the significant air and moisture sensitivities of this class of ionic liquid would be a disadvantage for many industrial applications. To alleviate these problems, environmentally stable ionic liquids were employed for the electrodeposition of silver from various salts at different substrates to generate either isolated nanoparticles or continuous thin films, depending on the electrodeposition parameters. The ILs studied have included 1-butyl-3-methylimidazolium tetrafluoroborate ([BMIm][BF₄]) [3,11], 1-butyl-3-methylimidazolium hexafluorophosphate ([BMIm][PF₆]) [11,12], 1-ethyl-3-methylimidazolium tetrafluoroborate ([EMIm][BF₄]) [13], 1-butyl-3-methylimidazolium bis(trifluoromethanesulfonyl)imide ([BMIm][TFSI]) [14], N-butyl-N-methyl-pyrrolidinium bis(trifluoromethanesulfonyl)imide

* Corresponding author.

** Corresponding author. Tel.: +61 3 99259940; fax: +61 3 9925 3747.

E-mail addresses: anand.bhatt@csiro.au (A.I. Bhatt),

anthony.omullane@rmit.edu.au (A.P. O'Mullane).

¹ ISE member.

([C₄mPyr][TFSI]) [15], N-butyl-N-methyl-pyrrolidinium dicyanamide ([C₄mPyr][DCA]) [15], DIMCARB [16] and 1-butyl-3-methylimidazolium trifluoromethylsulfonate ([BMIm][OTf]) [4]. However, to date few studies have systematically investigated the influence of the properties of the ionic liquid on the silver electrodeposition process [11]; instead, most studies have concentrated on end applications.

In this work we report on the electrodeposition of silver from commercially available ILs such as [BMIm][BF₄] and N-butyl-N-methyl-pyrrolidinium bis(trifluoromethanesulfonyl)imide ([C₄mPyr][TFSI]) using readily available silver salts such as AgBF₄ and AgOTf, and also an aqueous KNO₃ solution containing AgNO₃ as a comparison. We have chosen the IL [C₄mPyr][TFSI] given its lower reported viscosity than BF₄⁻ and PF₆⁻ based ILs, which for the latter also have the disadvantage of decomposing to produce hazardous species such as HF [17]. Given that industrial applications cannot be carried out on a large scale under inert atmosphere conditions without significantly increasing costs, we have also investigated the influence of atmospheric water uptake in [C₄mPyr][TFSI] to probe the influence that it may have on the silver electrodeposition process. Cyclic voltammetric and chronoamperometric methods are used to elucidate the deposition mechanism and the electrodeposits are characterised by scanning electron microscopy (SEM) and X-ray diffraction (XRD) to probe the significant solvent influence on the electrodeposition process.

2. Experimental

2.1. Materials

AgOTf (Sigma), AgBF₄ (Aldrich), AgNO₃ (Merck), ferrocene (Aldrich), [C₄mPyr][TFSI] (Merck), and [BMIm][BF₄] (Io-Li-Tec) were used as received. Aqueous solutions of 0.1 M KNO₃ (Ajax) were made up with deionized water (resistivity of 18.2 MΩ cm) purified by use of a Milli-Q reagent deioniser (Millipore). Ionic liquids and AgOTf were stored in a high purity Ar atmosphere glovebox (less than 5 ppm H₂O) when not in use.

2.2. Electrochemical measurements

Voltammetric experiments were conducted at 20 ± 2 °C with a CH Instruments (CHI 760C) electrochemical analyser in an electrochemical cell that allowed reproducible positioning of the working, reference, and auxiliary electrodes and a nitrogen inlet tube. A 0.0707 cm² glassy carbon (GC) electrode (BAS) was used as the working electrode. Prior to electrodeposition the electrode was polished with an aqueous 0.3 μm alumina slurry on a polishing cloth (Microcloth, Buehler), thoroughly rinsed with Milli-Q water, and dried with a flow of nitrogen gas. The reference electrode was Ag/AgCl (aqueous 3 M KCl) for experiments carried out in aqueous solution and an Ag/Ag⁺ (10 mM AgOTf in [C₄mPyr][TFSI]) for experiments carried out in [C₄mPyr][TFSI] [18]. In the case of experiments carried out in [BMIm][BF₄] a quasi silver reference electrode was employed in order to minimise junction potentials arising from use of the Ag/Ag⁺ (10 mM AgOTf in [C₄mPyr][TFSI]). For electrodeposition experiments a GC electrode was used as the working electrode and a platinum wire (BAS) as the counter electrode. All electrochemical experiments were commenced after degassing the electrolyte solutions with nitrogen for at least 10 min prior to any measurement.

2.3. Physical characterisation

Scanning electron microscopy (SEM) measurements were performed on an FEI Nova SEM (Philips) instrument with an AMETEK energy dispersive X-ray (EDX) system (Nova 200) operated at an

accelerating voltage of 30 kV. Imaging of solids deposited on the 3 mm GC electrodes was performed with the aid of a custom built electrode holder. Prior to SEM imaging, samples were thoroughly rinsed with acetone and Milli-Q water and dried under a flow of nitrogen. X-ray diffraction data were obtained with an AXS D8: Discovery (Bruker) with General Area Detector Diffraction System (GADDS). Samples for transmission electron microscopy (TEM) analysis were prepared by drop-casting the samples onto a carbon coated copper grid and performed using a 1010 TEM instrument (JEOL) operated at an accelerating voltage of 100 kV. UV/vis spectroscopy measurements of solutions were performed using a Cary 50 Bio-spectrophotometer (Varian). The moisture content for all ILs used in this study were determined using Karl Fischer titration.

3. Results and discussion

3.1. Cyclic voltammetry studies

A typical cyclic voltammogram for 20 mM AgBF₄ in [BMIm][BF₄] (water content 1960 ppm) recorded at a GC electrode using a scan rate of 50 mV s⁻¹ is shown in Fig. 1a. The voltammogram was scanned from 0.5 V to -0.9 V prior to switching of the scan direction. The voltammetric peak profiles are consistent with that expected for metal deposition and stripping from an electrode surface [19]. On the negative sweep the electrodeposition of Ag⁺ commences at -0.220 V vs Ag QRE until the cathodic current reaches a maximum at -0.39 V, after which the current attains a diffusion limited value until the end of the sweep at -0.90 V. On the reverse sweep a current crossover is observed at -0.30 V which is indicative of a nucleation-growth mechanism [4,11,20] after which a broad oxidative stripping peak is observed at 0.16 V. This also indicates that the electrodeposition of Ag on GC requires an overpotential to initiate the nucleation and growth of bulk silver. Also shown in Fig. 1b is the scan rate dependence on the electrodeposition process, where a plot of peak current as a function of the square root of scan rate exhibits a linear dependence over a scan rate range of 50–500 mV s⁻¹, as expected for a diffusion controlled process. The small intercept that is observed is most likely due to changes in the electrode area as silver is being deposited, as was observed previously for the electrodeposition of Ag on GC from DIMCARB [16]. As shown in Table 1, the shift in E_p^{red} to more negative potentials on increasing the scan rate is again indicative of a nucleation-growth process [21] whereas the electrodisolution potential, E_p^{ox}, of silver from the GC surface shows significantly less dependence on sweep rate; only a shift of 26 mV is observed over the scan rate range of 50–500 mV s⁻¹.

Fig. 1c shows a typical voltammogram recorded at a GC electrode for a solution of 10 mM AgOTf in dry [C₄mPyr][TFSI] at 50 mV s⁻¹ (60 ppm water content). On the negative sweep, electrodeposition commences at -0.15 V vs Ag/Ag⁺ reference electrode and reaches a maximum at -0.20 V, after which a diffusion limited current is attained until the end of the sweep. On the reverse sweep a current crossover is observed at -0.16 V indicative of a nucleation and growth process which is followed by an oxidative stripping peak at 0.14 V. The observed shift in E_p^{red} to more negative potentials on increasing the scan rate is again suggestive of a nucleation-growth process (Table 1). The plot of peak current as a function of the square root of scan rate (Fig. 1d) exhibits a linear dependence over a scan rate range of 50–500 mV s⁻¹. As observed in the previous case an intercept is present in the plot of peak current vs square root of scan rate. This intercept is markedly larger than that observed in the case of [BMIm][BF₄] and the excess current is attributed to a combination of growth in electrode area due to silver electrodeposition and chemical reaction occurring between the silver cation and ionic liquid. This type of behaviour has previously been observed in the case

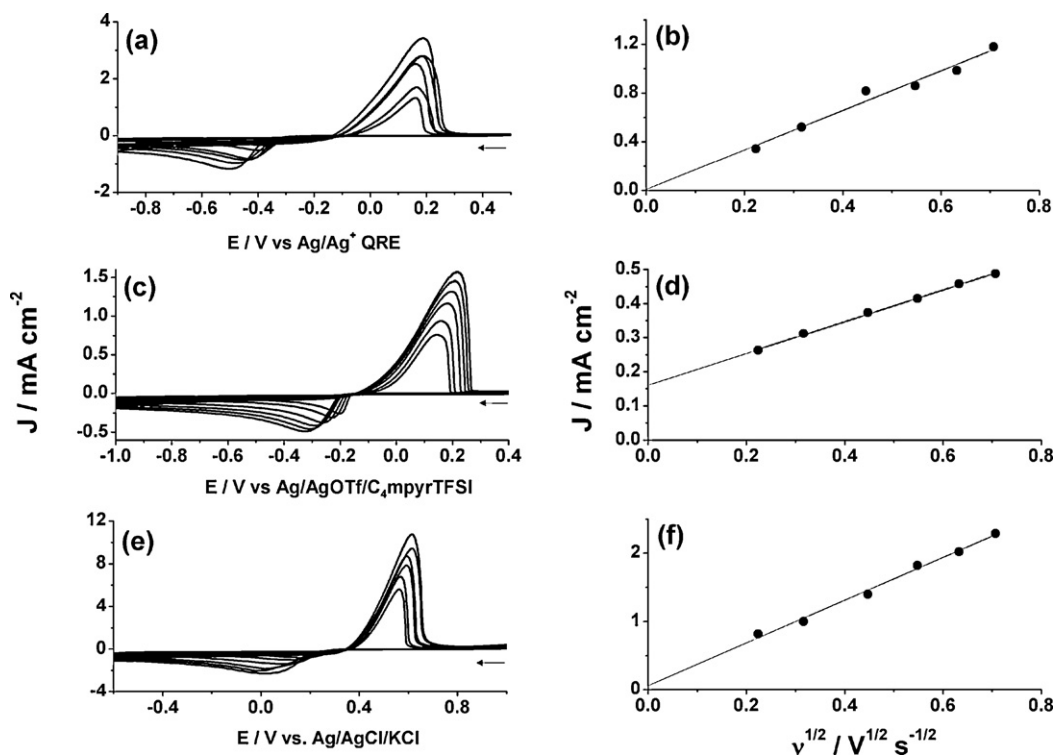


Fig. 1. Cyclic voltammograms for reduction of Ag^+ to Ag onto GC electrodes at a scan rate range of 50 to 500 mV s^{-1} : (a) 20 mM AgBF_4 in $[\text{BMIm}][\text{BF}_4]$ and (b) plot of deposition current as function of square root of scan rate; (c) 10 mM AgOTf in dry $[\text{C}_4\text{mPyr}][\text{TFSI}]$ and (d) plot of deposition current as function of square root of scan rate; and (e) 5 mM AgNO_3 in 0.1 M KNO_3 and (f) plot of deposition current as function of square root of scan rate. All CVs measured at 20 °C under inert atmosphere.

of a distillable ionic liquid, DIMCARB [16] and is detailed further in the following section.

Typical voltammograms obtained for the deposition of silver from 10 mM AgNO_3 in 0.1 M KNO_3 are shown in Fig. 1e. The onset

potential for electrodeposition of silver is 0.36 V vs Ag/AgCl with a current maximum at 0.16 V, after which a steady state current is observed until the end of the sweep at -0.60 V. On the positive sweep a current crossover is observed at 0.30 V and the reduction

Table 1

Cyclic voltammetric data obtained for reduction of Ag^+ to Ag onto GC electrodes from 20 mM AgBF_4 in $[\text{BMIm}][\text{BF}_4]$, 10 mM AgOTf in dry $[\text{C}_4\text{mPyr}][\text{TFSI}]$, 10 mM AgOTf in wet $[\text{C}_4\text{mPyr}][\text{TFSI}]$ and 5 mM AgNO_3 in 0.1 M KNO_3 at 20 °C under inert atmosphere. Voltammetric data^a obtained as a function of sweep rate.

Scan rate (mV s^{-1})	E_p^{red} (V)	E_p^{ox} (V)	E_m (V)	$\Delta E_p^{\text{ox-red}}$ (V)	Q_{red} (mC)	Q_{ox} (mC)	$Q_{\text{ox}}/Q_{\text{red}}$
Electrodeposition of silver onto a GC electrode from a solution containing 20 mM AgBF_4 in $[\text{BMIm}][\text{BF}_4]$							
50	-0.386	0.161	-0.113	0.547	0.24	0.22	0.92
100	-0.395	0.164	-0.116	0.559	0.20	0.19	0.95
200	-0.430	0.162	-0.134	0.592	0.16	0.15	0.94
300	-0.445	0.184	-0.131	0.629	0.12	0.12	1.00
400	-0.479	0.186	-0.147	0.665	0.10	0.10	1.00
500	-0.501	0.187	-0.157	0.688	0.10	0.09	0.90
Electrodeposition of silver onto a GC electrode from a solution containing 10 mM AgOTf in dry $[\text{C}_4\text{mPyr}][\text{TFSI}]$ (water content of 60 ppm)							
50	-0.201	0.216	0.008	0.417	0.16	0.15	0.94
100	-0.228	0.208	-0.010	0.436	0.10	0.10	1.00
200	-0.261	0.197	-0.032	0.458	0.07	0.07	1.00
300	-0.290	0.179	-0.056	0.469	0.06	0.06	1.00
400	-0.306	0.160	-0.073	0.466	0.05	0.05	1.00
500	-0.323	0.144	-0.090	0.467	0.05	0.04	0.80
Electrodeposition of silver onto a GC electrode from a solution containing 10 mM AgOTf in wet $[\text{C}_4\text{mPyr}][\text{TFSI}]$ (water content of 460 ppm)							
50	-0.673	-0.109	-0.283	0.783	5.09×10^{-3}	4.10×10^{-3}	0.81
100	-0.756	-0.113	-0.322	0.869	6.86×10^{-3}	5.57×10^{-3}	0.81
200	-0.851	-0.178	-0.337	1.029	8.93×10^{-3}	8.10×10^{-3}	0.91
300	-0.881	-0.176	-0.353	1.057	11.3×10^{-3}	9.91×10^{-3}	0.87
400	-0.930	-0.162	-0.384	1.092	12.6×10^{-3}	10.9×10^{-3}	0.86
500	-0.968	-0.117	-0.423	1.085	14.3×10^{-3}	12.2×10^{-3}	0.86
Electrodeposition of silver onto a GC electrode from a solution containing 5 mM AgNO_3 in 0.1 M KNO_3							
50	0.164	0.563	0.364	0.399	1.00	0.88	0.88
100	0.109	0.569	0.339	0.460	0.64	0.56	0.88
200	0.082	0.592	0.337	0.510	0.42	0.39	0.93
300	0.023	0.594	0.309	0.571	0.35	0.29	0.83
400	0.004	0.615	0.310	0.611	0.30	0.26	0.87
500	0.016	0.615	0.316	0.599	0.27	0.24	0.89

^a E_m represents the midpoint potential measured as $(E_p^{\text{red}} + E_p^{\text{ox}})/2$ in volts vs the relevant reference electrode. E_p^{red} and E_p^{ox} are reduction and oxidation peak potentials, respectively; Q_{red} and Q_{ox} are the charges associated with the reduction and oxidation processes.

peak potential shifts to less positive potentials on increasing the scan rate, indicating again a nucleation–growth process. The broad oxidative stripping peak at 0.56 V remains largely unaffected by increasing sweep rate. The reduction peak current is proportional to the square root of scan rate (Fig. 1f) indicating a diffusion controlled process, again with the observation of a non zero intercept due to concomitant changes in electrode area from deposition of a conductive metal.

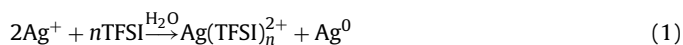
In the case of the aqueous solution, the ratio of the charge associated with the stripping process to the reduction process, Q_{ox}/Q_{red} , is always less than one (Table 1), which indicates that the removal of silver from a GC surface is not a fully chemically reversible process. However, in the case of both ionic liquids nearly full chemical reversibility is seen for silver deposition/stripping (Table 1). The oxidative removal of silver in the aqueous solution at pH = 5.4 may be complicated due to the formation of some surface oxides on silver during the oxidation sweep and may account for the lack of full chemical reversibility. This is observed in Fig. 2 where CVs are obtained using a silver electrode at different pH values. In 1 M H_2SO_4 , pH = 0.45 (Fig. 2a), the anodic current clearly increases without the appearance of any peak maximum due to dissolution of Ag to Ag^+ . When this experiment is performed in 1 M NaOH, pH = 13 (Fig. 2b) it can be seen clearly that there are peaks associated with the formation of oxides on the silver surface [22]. Under the conditions of our electrodeposition experiments which were carried out in 0.1 M KNO_3 , pH = 5.4 (Fig. 2c) it can be seen that there is a distinct anodic peak prior to the onset of bulk dissolution of Ag into Ag^+ which indicates some oxide formation. This may be the origin of the lack of chemical reversibility seen in the aqueous case for silver deposition/stripping.

3.1.1. Influence of water content on silver electrodeposition in $[C_4mPyr][TFSI]$

In all cases the electrodeposition of silver is sensitive to the nature of the electrode surface, which can be alleviated through rigorous polishing procedures. However, in the case of $[C_4mPyr][TFSI]$ it was found that performing the silver electrodeposition experiments on the bench rather than under dry glovebox conditions resulted in significantly different electrochemical behaviour. After exposure of the AgOTf in $[C_4mPyr][TFSI]$ electrolyte to ambient conditions, it was noticed during CV experiments that sometimes a shoulder appeared with the main deposition process during the reduction sweep (data not shown). If CVs are recorded after full atmospheric water absorption occurs (460 ppm H_2O content) in the 'wet' $[C_4mPyr][TFSI]$, significant differences in the voltammetry can be observed (Fig. 3). Firstly, the reduction process due to $Ag^+ \rightarrow Ag^0$ reaction is shifted ca. 400 mV to more negative potentials. Secondly, a significant decrease in current density is observed. Thirdly, two shoulders are observed in addition to the main reduction process. These are attributed to the reduction of Ag^{2+} and deposition of Ag onto adsorbed silver nanoparticles on the GC surface (see below for discussion). Similar behaviour has been observed previously for Ag electrodeposition from DIMCARB on GC, where two reduction processes were observed and attributed to the reduction of silver on GC and silver on silver nanoparticles adsorbed on the electrode and formed chemically from the slow reaction of DIMCARB with silver ions [16]. Additionally, in that study a shifting of the reduction potential by up to 1 V was observed due to the effect of nanoparticle adsorption onto the GC surface. If the silver/ $[C_4mPyr][TFSI]$ electrolyte solution is left for sufficient time then only a single deposition process is observed, however, the deposition potential is significantly shifted to further negative potentials. It can also be seen that the Q_{ox}/Q_{red} ratio is less than one (Table 1) and is similar to the case of silver deposition and stripping from aqueous solution and suggests that the presence of atmospheric water impacts on the chemical reversibility of the system by the possible forma-

tion of surface oxides. Similar to the aqueous system, CVs of silver electrodes in $[C_4mPyr][TFSI]$ show presence of surface oxides in the wet IL (Fig. 2d). Interestingly in the case of the dry IL (Fig. 2d) this behaviour is not replicated and only anodic dissolution of Ag^0 to Ag^+ is observed. This implies that silver oxide formation in the IL system only occurs if sufficient water is present.

The observation that silver nanoparticles are chemically formed from AgOTf in $[C_4mPyr][TFSI]$ was also experimentally observed by UV/vis spectroscopy (Fig. 4a), which clearly shows a surface plasmon resonance feature at 483 nm indicative of silver nanoparticle formation [23,24]. The presence of Ag nanoparticles was also confirmed by TEM imaging (Fig. 4b), EDX analysis during SEM imaging and XRD measurements which showed reflections due to fcc silver. This phenomenon was observed after exposure of the electrolyte solution to atmosphere after ca. 1 h but was only observed under inert conditions after a time period of greater than 5 h. This is most likely related to the water content of the IL, which was found to be 60 ppm under glovebox conditions and 460 ppm under benchtop conditions using Karl Fischer measurements. These values are in close agreement with those obtained by Compton for the same IL [25]. It should be noted that silver solutions prepared and stored in the dark also formed nanoparticles in a similar timeframe which discounts the possibility that nanoparticle formation is occurring from reaction with UV radiation from sunlight. This finding suggests that the nanoparticle formation mechanism is related to the reaction of Ag^+ with electrolyte moieties rather than the effects of direct UV irradiation. The nature of the chemical interaction between silver ions and the IL moieties is not clear at present. It has been shown previously that monovalent Cu^+ and Ag^+ ions can disproportionate to form the M^{2+} ion and M^0 in the presence of water and chelating ligands such as 5,5,7,12,12,14-hexamethyl-1,4,8,11-tetraazacyclotetradecane (ligand L) [26]. Since Ag^+ is known to be chelated/coordinated by the TFSI anion [27] we hypothesise that a similar reaction mechanism may be occurring as shown by the following reaction:



UV/vis spectra of $[C_4mPyr][TFSI]$ after reaction to form the nanoparticles and subsequent removal of the nanoparticles by centrifugation show a broad band centred at ca. 350 nm (Fig. 4a). Previously, it has been shown that the d–d transition for Ag^{2+} is in the region of 348–376 nm [28]. The spectral data obtained tentatively supports the disproportionation theory for formation of Ag^0 by Reaction (1).

The voltammetric response of the Ag^{2+}/Ag^+ couple has been previously explored and is found to be at more negative potentials compared to the Ag^+/Ag^0 process. Based on these results the small shoulder observed in Fig. 3 at -0.930 V may be attributed to Ag^{2+} reduction, further supporting the disproportionation theory. The 255 mV peak–peak separation is close to that of ca. 250 mV reported by Sroczynski and Grzejdziaik for Ag^{2+} isocyclam complexes in aqueous solution [28]. Based on this analysis the final process at -1.190 V is then attributed to the reduction of Ag^+ to Ag^0 onto silver nanoparticles which are adsorbed onto the GC surface as also observed previously in the case of Ag^+ reduction from DIMCARB [16].

It has been shown that the disproportionation reaction in wet organic solvents in the presence of the chelating ligand, L, produces a mirror on the walls of the reaction vessel [26], that is bulk formation of silver metal occurs. It has also been shown that in dry solvents, i.e., in the absence of water, this reaction does not occur [26]. Since the ILs used in the study have low to moderate levels of water impurity, combined with a chelating ligand (TFSI anion) the disproportionation reaction can occur. Presumably, the higher viscosity of the IL and/or lower equilibrium constants results in slower

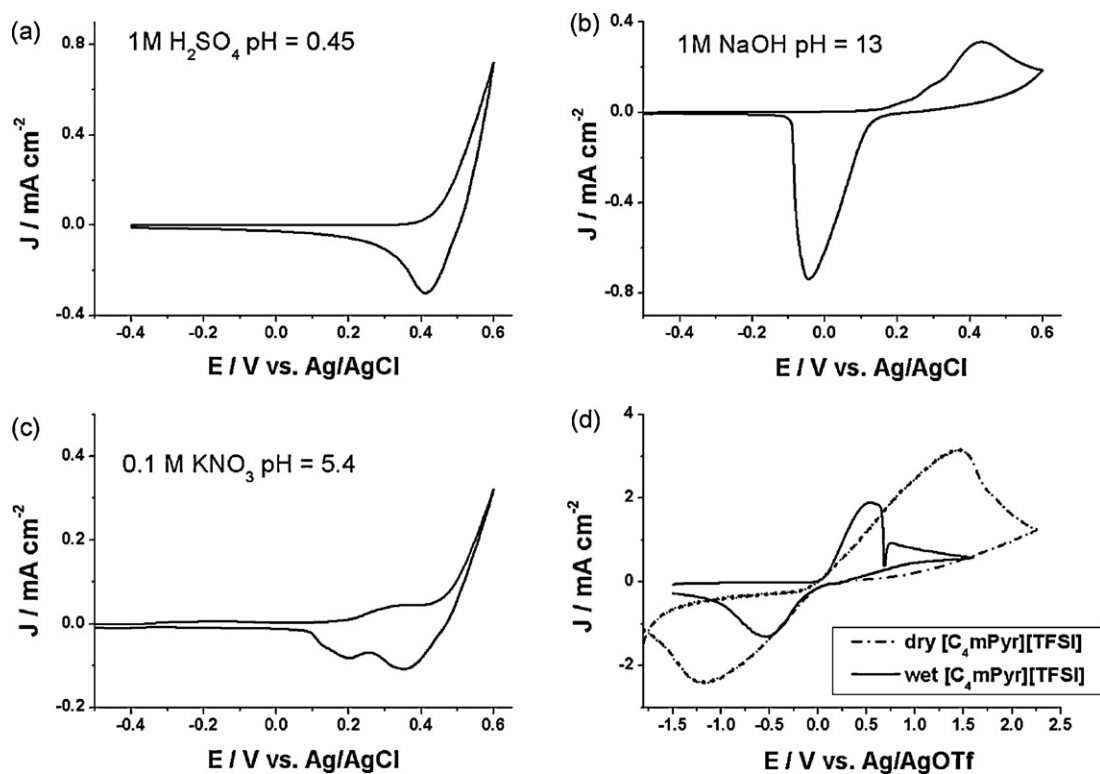


Fig. 2. Cyclic voltammograms obtained for a silver electrode in 1 M H₂SO₄ (pH = 0.45), 1 M NaOH (pH = 13) and 0.1 M KNO₃ (pH = 5.4) measured at 20 °C and a scan rate of 0.05 V s⁻¹.

formation of the silver metal and thus enables nanoparticles to be formed as opposed to bulk metallic silver. If the [C₄mPyr][TFSI]/Ag⁺ solution is left in a sealed vessel for a long time period (4 weeks) the eventual formation of a silver deposit on the walls of the vessel does occur due to the eventual diffusion and combination of the reactive nanoparticles to form the bulk metal.

In light of the fact that silver nanoparticles are formed under ambient conditions (with associated voltammetric changes), and given that the reference electrode employed was an Ag/Ag⁺ (10 mM silver triflate in [C₄mPyr][TFSI]) [18] the stability of the reference electrode was also tested under glovebox conditions and on the bench using ferrocene as a redox probe. It was found that there was

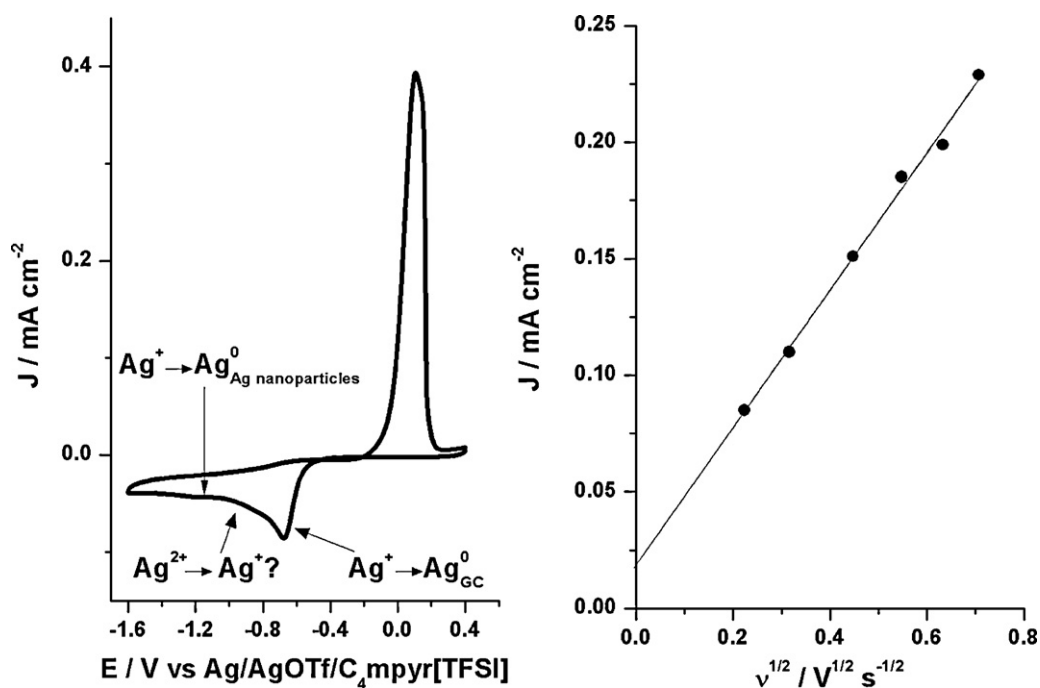


Fig. 3. (a) Cyclic voltammogram of 10 mM AgOTf in wet [C₄mPyr][TFSI] measured at 20 °C under inert atmosphere using a scan rate of 0.05 V s⁻¹ and (b) plot of deposition current as a function of square root of scan rate.

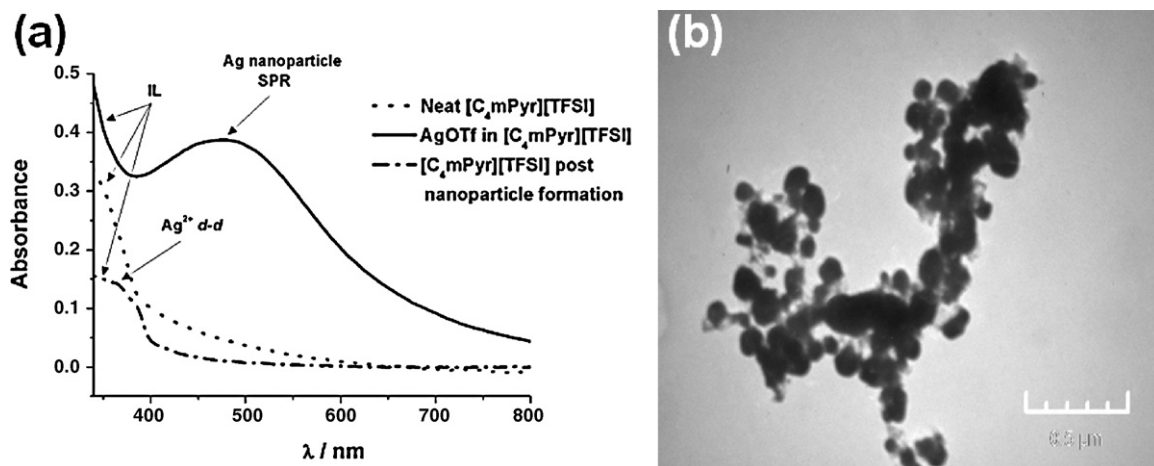


Fig. 4. (a) UV/vis spectra of 10 mM AgOTf in [C₄mPyr][TFSI] (—) recorded 24 h after dissolution, also shown neat [C₄mPyr][TFSI] (···) and [C₄mPyr][TFSI] after removal of nanoparticles by centrifugation; (b) TEM images of silver nanoparticles formed by chemical reduction of Ag⁺ in [C₄mPyr][TFSI].

no difference in the E^0 value recorded for the ferrocene/ferrinium process under these different conditions. This therefore suggests that the shifts in the onset for silver electrodeposition are related to the nature of the electrode surface. Previously Snook et al. have commented upon the stability of this reference electrode under inert conditions [18], and it would appear that the reference also shows stability under ambient conditions.

3.2. Chronoamperometry

Chronoamperometry was employed to probe the nucleation and growth mechanism suggested by the voltammetric data. Chronoamperograms were recorded at a GC electrode and the potential was stepped from an initial value where no deposition occurs to successively negative potential values close to E_p^{red} and beyond. Typical chronoamperograms obtained are shown in Fig. 5. In all cases the $J-t$ curves for potential values close to E_p^{red} show an initial current maximum J_m at time t_m , which then quickly decays to a diffusion limited current. At potentials sufficiently negative from E_p^{red} the current response is described by the well-known $t^{-1/2}$ Cottrellian decay and no current maximum is observed.

A number of models have been developed to describe the $J-t$ curves for metal electrodeposition. It has been shown previously that the theoretical methodology developed by Scharifker and Hills [29] is applicable to deposition from IL media [16,30,31]. It has been previously reported by Milchev et al. during metal electrodeposition in the absence of supporting electrolyte, when ion migration effects become prominent, that substantially different $J-t$ curves are observed [32]. However, in the case of ionic liquids the concentration of ions is higher than that in aqueous systems which negates the possibility of any ion migration effects. Indeed the $J-t$ curves are typical for that found for a 3D nucleation and growth process without interference from ohmic, diffusion or ion transfer limitations. Therefore, in this study the Hills–Scharifker treatment was applied which describes two limiting cases, progressive and instantaneous growth mechanisms, for the initial stages of 3D nucleation and 2D growth of deposited nuclei. In the case of progressive nucleation where the initially deposited adatoms grow at varying rates dependent on time of deposition, the $J-t$ curves can be mathematically described by the following equation.

For 3D progressive nucleation and 2D growth:

$$\left(\frac{J}{J_m}\right)^2 = \frac{1.2254}{t/t_m} \left\{ 1 - \exp \left[-2.3367 \left(\frac{t}{t_m}\right)^2 \right] \right\}^2 \quad (2)$$

where J is the current density at time t and J_m is the maximum current density at time t_m .

In the case of instantaneous nucleation adatoms are deposited onto the electrode surface and grow at a constant rate that is dependent on the applied potential. The resultant $J-t$ curves are mathematically described by the following equation.

For 3D instantaneous nucleation and 2D growth:

$$\left(\frac{J}{J_m}\right)^2 = \frac{1.9542}{t/t_m} \left\{ 1 - \exp \left[-1.2564 \left(\frac{t}{t_m}\right) \right] \right\}^2 \quad (3)$$

Additional information regarding the silver diffusion coefficient and number of nuclei on the electrode surface can also be extrapolated from the CA data using the Hills–Scharifker methodology, which is described by the following Eqs. (4)–(9). Data calculated using Eqs. (4)–(9) are shown in Table 2 for all of the systems used in this study.

In the case of progressive nucleation:

$$t_m = \left(\frac{4.6733}{AN_\infty \pi k' D} \right)^{1/2} \quad (4)$$

$$J_m = 0.4615 nFD^{3/4} C_{\text{bulk}} (k' AN_\infty)^{1/4} \quad (5)$$

$$I_m^2 t_m = 0.2598 (nFC_{\text{bulk}})^2 D \quad (6)$$

$$t_m = \frac{1.2564}{N\pi kD} \quad (7)$$

$$J_m = 0.6382 nFDC_{\text{bulk}} (kN)^{1/2} \quad (8)$$

$$J_m^2 t_m = 0.1629 (nFC_{\text{bulk}})^2 D \quad (9)$$

where N is the number of nuclei, D is the diffusion coefficient, C_{bulk} is the bulk concentration, $k = (8\pi C_{\text{bulk}} M/\rho)^{1/2}$ (M is the molar mass of the depositing species and ρ is the density of depositing species) and $k' = (4/3)(8\pi C_{\text{bulk}} M/\rho)^{1/2}$.

Typical $J-t$ curves obtained for AgBF₄ reduction in [BMIm][BF₄] (presented as non-dimensional plots) are shown in Fig. 5a with the theoretical curves predicted by Eqs. (2) and (3). These results are typical of this analysis of the experimental responses observed in this study as can be seen for the case of [C₄mPyr][TFSI] where the original experimental $J-t$ curves are illustrated (in Fig. 5e). As can be observed, the best fit of the data suggests that Ag⁺ is reduced and deposited onto the GC electrode surface via an instantaneous mechanism. The results presented in this study show good correlation with the theoretical curves. This is in contrast to similar experiments performed by He et al. [11] where the chronoamperometry data showed intermediate behaviour attributed to nuclei growth

Table 2

Chronoamperometric data obtained for reduction of Ag^+ to Ag onto GC electrodes from 20 mM AgBF_4 in $[\text{BMIm}][\text{BF}_4]$, 10 mM AgOTf in dry $[\text{C}_4\text{mPyr}][\text{TFSI}]$, 10 mM AgOTf in wet $[\text{C}_4\text{mPyr}][\text{TFSI}]$ and 5 mM AgNO_3 in 0.1 M KNO_3 at 20 °C under inert atmosphere.

E_{step} (V)	t_m (s)	J_m (A cm^{-2})	$J_m^2 t_m$ ($\text{A}^2 \text{cm}^{-4} \text{s}$)	D ($\text{cm}^2 \text{s}^{-1}$)
20 mM AgBF_4 in $[\text{BMIm}][\text{BF}_4]$				
-0.25	1.4	2.1×10^{-4}	6.5×10^{-8}	1.1×10^{-8}
-0.30	0.4	2.2×10^{-4}	1.9×10^{-8}	3.1×10^{-8}
-0.35	0.4	2.9×10^{-4}	3.4×10^{-8}	5.6×10^{-8}
				Calculated D : $6.5 \pm 2.8 \times 10^{-8}$
10 mM AgOTf in dry $[\text{C}_4\text{mPyr}][\text{TFSI}]$				
-0.25	0.5	1.1×10^{-4}	5.7×10^{-9}	2.4×10^{-8}
-0.30	1.3	1.3×10^{-4}	2.2×10^{-8}	9.0×10^{-8}
-0.35	0.3	2.7×10^{-4}	2.3×10^{-8}	9.3×10^{-8}
-0.40	0.3	2.7×10^{-4}	2.2×10^{-8}	9.2×10^{-8}
-0.45	0.1	3.8×10^{-4}	1.5×10^{-8}	6.1×10^{-8}
				Calculated D : $2.6 \pm 1.7 \times 10^{-8}$
10 mM AgOTf in wet $[\text{C}_4\text{mPyr}][\text{TFSI}]$				
-0.50	1.1	1.2×10^{-4}	1.6×10^{-8}	6.8×10^{-8}
-0.55	0.5	1.4×10^{-4}	9.3×10^{-9}	3.8×10^{-8}
-0.60	0.03	1.8×10^{-4}	9.0×10^{-10}	3.7×10^{-9}
-0.65	0.3	1.9×10^{-4}	1.0×10^{-8}	4.2×10^{-8}
-0.70	0.2	2.8×10^{-4}	1.2×10^{-8}	5.0×10^{-8}
-0.75	0.1	3.4×10^{-4}	1.3×10^{-8}	5.2×10^{-8}
-0.80	0.1	2.9×10^{-4}	1.1×10^{-8}	4.7×10^{-8}
-0.85	0.1	2.9×10^{-4}	1.1×10^{-8}	4.4×10^{-8}
-0.90	0.06	3.5×10^{-4}	8.0×10^{-9}	5.3×10^{-8}
-0.95	0.08	3.1×10^{-4}	8.4×10^{-9}	5.6×10^{-8}
-1.00	0.09	3.4×10^{-4}	1.1×10^{-8}	4.5×10^{-8}
-1.05	0.06	4.3×10^{-4}	1.2×10^{-8}	5.0×10^{-8}
-1.10	0.04	5.2×10^{-4}	1.1×10^{-8}	4.5×10^{-8}
-1.15	0.04	4.2×10^{-4}	7.7×10^{-9}	3.2×10^{-8}
				Calculated D : $4.5 \pm 0.9 \times 10^{-8}$
5 mM AgNO_3 in 0.1 M KNO_3				
0.35	0.5	7.8×10^{-4}	3.3×10^{-7}	8.6×10^{-6}
0.30	0.02	2.2×10^{-3}	1.2×10^{-7}	3.1×10^{-6}
0.25	0.006	6.7×10^{-3}	2.6×10^{-7}	6.9×10^{-6}
0.20	0.1	2.3×10^{-3}	5.0×10^{-7}	1.3×10^{-5}
0.15	0.06	2.8×10^{-3}	4.9×10^{-7}	1.3×10^{-5}
0.10	0.05	3.3×10^{-3}	6.2×10^{-7}	1.6×10^{-5}
0.05	0.04	3.9×10^{-3}	6.6×10^{-7}	1.7×10^{-5}
0.00	0.06	3.9×10^{-3}	9.5×10^{-7}	2.5×10^{-5}
-0.05	0.05	4.2×10^{-3}	1.0×10^{-6}	2.7×10^{-5}
-0.10	0.03	5.5×10^{-3}	1.0×10^{-6}	2.7×10^{-5}
-0.15	0.02	6.9×10^{-3}	9.6×10^{-7}	2.5×10^{-5}
-0.20	0.01	9.4×10^{-3}	8.8×10^{-7}	2.3×10^{-5}
-0.25	0.008	1.1×10^{-2}	9.5×10^{-7}	2.5×10^{-5}
-0.30	0.006	1.3×10^{-2}	1.0×10^{-6}	2.7×10^{-5}
				Calculated D : $1.8 \pm 0.7 \times 10^{-5}$

controlled by both mixed kinetics and diffusion [11,33]. We note that He et al. used dried $[\text{BMIm}][\text{BF}_4]$ and a higher Ag^+ concentration [11] whereas the IL used in this study was not further purified from supplier specifications. Clearly, the combined effects of water impurity from atmospheric absorption and lowering the Ag^+ concentration serves to reduce the mixed kinetic effects noted by He et al. [11], resulting in instantaneous behaviour. The instantaneous nature of deposition has also been confirmed by SEM analysis (see Section 3.3).

Due to the Ag nanoparticle formation reaction in $[\text{C}_4\text{mPyr}][\text{TFSI}]$, the chronoamperometric data was measured as a function of either dried or wet (from absorption of atmospheric water) IL. In both cases the data was recorded immediately after dissolution of the silver salt in the IL. This minimised the effects on the electrochemistry results from contributions due to the coupled chemical reaction that causes nanoparticle formation. It has previously been shown that electrochemical measurements can be made when silver nanoparticle chemical formation occurs if the data collection time is short compared to the nanoparticle formation time [16]. However, some care should be taken when interpreting results as contributions from a coupled chemical process cannot be entirely discounted.

In the case of dry $[\text{C}_4\text{mPyr}][\text{TFSI}]$ the non-dimensional J - t curves are shown in Fig. 5b. As was also found for the case of $[\text{BMIm}][\text{BF}_4]$,

the best fit of the data suggests an instantaneous mechanism. However, significant differences in behaviour are observed if the dry IL is allowed to absorb moisture from the atmosphere. Plots of the J - t curves in this case are shown in Fig. 5c and the data is best described by the theoretical transients for progressive nucleation and growth. Clearly, the effect of water impurity on this deposition reaction is significant enough to change the initial silver deposition mechanism. These mechanistic changes are also highlighted in the deposit morphologies as shown in the SEM images (see Section 3.3). Since care was taken to ensure that the contribution from chemically formed nanoparticles was minimal and that the deposition conditions were the same (including shielding from UV radiation), this mechanistic change is most likely the sole result of an increase in water content which may affect the interfacial double layer of the working electrode, kinetics of the electrodeposition process and viscosity of the ionic liquid.

Turning to the deposition of Ag from 0.10 M KNO_3 /water, the J - t curves are shown in Fig. 5d. The data obtained is strongly dependent on the deposition voltage. At potentials close to the onset potential for Ag deposition of 0.35 V the J - t curves are best fitted by the theoretical transients for instantaneous nucleation and growth. However, as the potential is successively stepped towards E_p^{red} (-0.15 V), the nature of the mechanism changes and tends towards progressive nucleation and growth. This phenomenon was

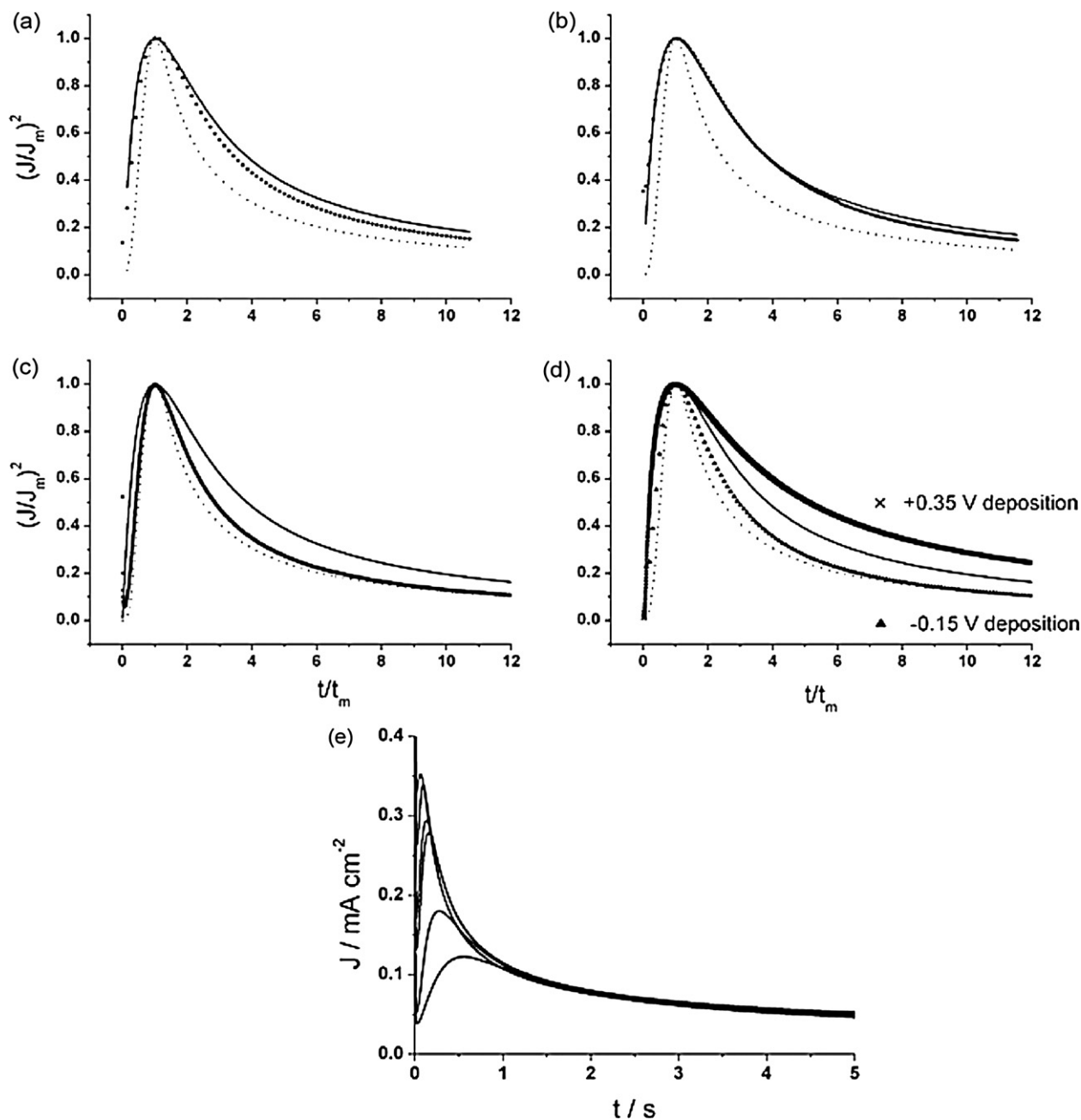


Fig. 5. Nondimensional plots of $(j/j_m)^2$ vs t/t_m for the electrodeposition of silver from (a) 20 mM AgBF_4 in $[\text{BMIm}][\text{BF}_4]$; (b) 10 mM AgOTf in dry $[\text{C}_4\text{mPyr}][\text{TFSI}]$; (c) 10 mM AgOTf in wet $[\text{C}_4\text{mPyr}][\text{TFSI}]$; (d) 5 mM AgNO_3 in 0.1 M KNO_3 . Overlaid are the theoretical curves calculated using Eqs. (2) and (3) for instantaneous (—) and progressive (···) nucleation and diffusion limited growth and (e) typical plots obtained of current vs time for 10 mM AgOTf in dry $[\text{C}_4\text{mPyr}][\text{TFSI}]$; shown data obtained at stepping potentials of 0.5–1.0 V in 0.1 V steps.

not observed in the case of Ag electrodeposition from $[\text{BMIm}][\text{BF}_4]$ and dry $[\text{C}_4\text{mPyr}][\text{TFSI}]$.

It has been shown previously that the number density of nuclei formed has a dependence on the overpotential applied. Gunawardena et al. have shown that the nucleation number density, N_0 , can be calculated from the rising portion of the J - t curves using the following relationship [34]:

$$J = \frac{1.04 n F \pi (2DC_{\text{bulk}})^{3/2} M^{1/2} N_0 t^{1/2}}{\rho^{1/2}} \quad (10)$$

During the initial stages of deposition, well before the maxima in the J - t curves, the initial nucleation can be considered to be effectively instantaneous [34]. This theory, proposed by Gunawardena et al. [34], analyses the deposited nuclei at an early stage when the

diffusion fields of the nuclei do not overlap. Thus, if care is taken to analyse data from the very early portion of the current transient, Eq. (10) can be used to estimate the value of N_0 for all the systems studied. Using this methodology we have estimated the number of nuclei formed during the very early stages of nucleation to allow trends to be ascertained between the different solvent systems studied.

A plot of N_0 calculated using Eq. (10) as a function of depositing voltage is shown in Fig. 6. In the case of the aqueous system the data shows that at overpotentials which lead to an eventual instantaneous nucleation mechanism, at voltages close to E_p^{red} , the initially high values of N_0 decay to lower values as E_p^{red} is approached. However, as the deposition overpotential voltage is increased into the region where an eventual progressive nucleation mechanism oper-

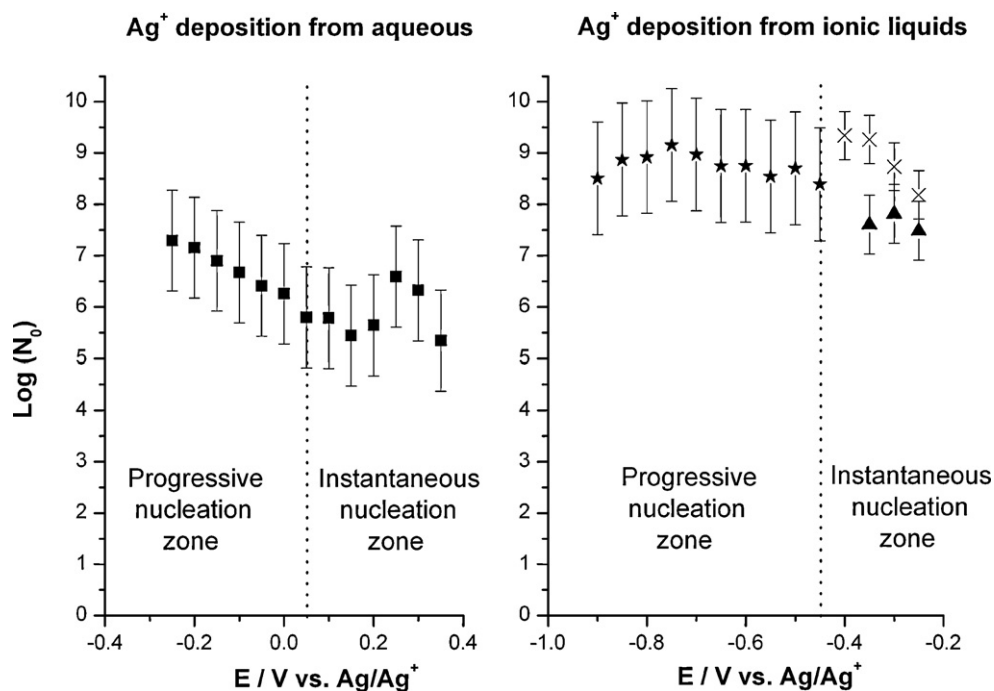


Fig. 6. Plot of nucleation number density (N_0) calculated using Eq. (10) as a function of applied potential for Ag deposition onto GC from 5 mM AgNO_3 in 0.1 M KNO_3 (left) and ionic liquids (right): 20 mM AgBF_4 in $[\text{BMIm}][\text{BF}_4]$ (\blacktriangle), 10 mM AgOTf in dry $[\text{C}_4\text{mPyr}][\text{TFSI}]$ (\times) and 10 mM AgOTf in wet $[\text{C}_4\text{mPyr}][\text{TFSI}]$ (\star).

ates, the values of N_0 begin to rise in a linear relationship. Given that Eq. (10) refers to the case of instantaneous nucleation at very short times it is interesting to correlate the number of nuclei formed at this short time scale. However, the number of nuclei calculated is only used to observe trends between the different solvent systems and is not taken as the absolute number of nuclei formed.

In the case of the ILs, the data for $[\text{C}_4\text{mPyr}][\text{TFSI}]$ show that high values of N_0 are observed for the dry IL, similar to the aqueous case. However, in the case of the wet IL, lower values of N_0 are observed that follow a linear relationship when a progressive

nucleation mechanism was predicted to operate after analysis of the full transient. The data for $[\text{C}_4\text{mPyr}][\text{TFSI}]$ would then appear to show a similar trend to the aqueous case if the effect of the water impurity is discounted. It is tentatively proposed that the effect of water addition to the IL is as follows. As water content is increased significantly, the physical properties of the IL change and a concomitant decrease in viscosity and hence increase in mass transport is obtained. This is reflected by the increase in the diffusion coefficient of Ag^+ from $2.6 \pm 1.7 \times 10^{-8}$ in dry $[\text{C}_4\text{mPyr}][\text{TFSI}]$ to $4.5 \pm 0.9 \times 10^{-8} \text{ cm}^2 \text{ s}^{-1}$ in $[\text{C}_4\text{mPyr}][\text{TFSI}]$ after

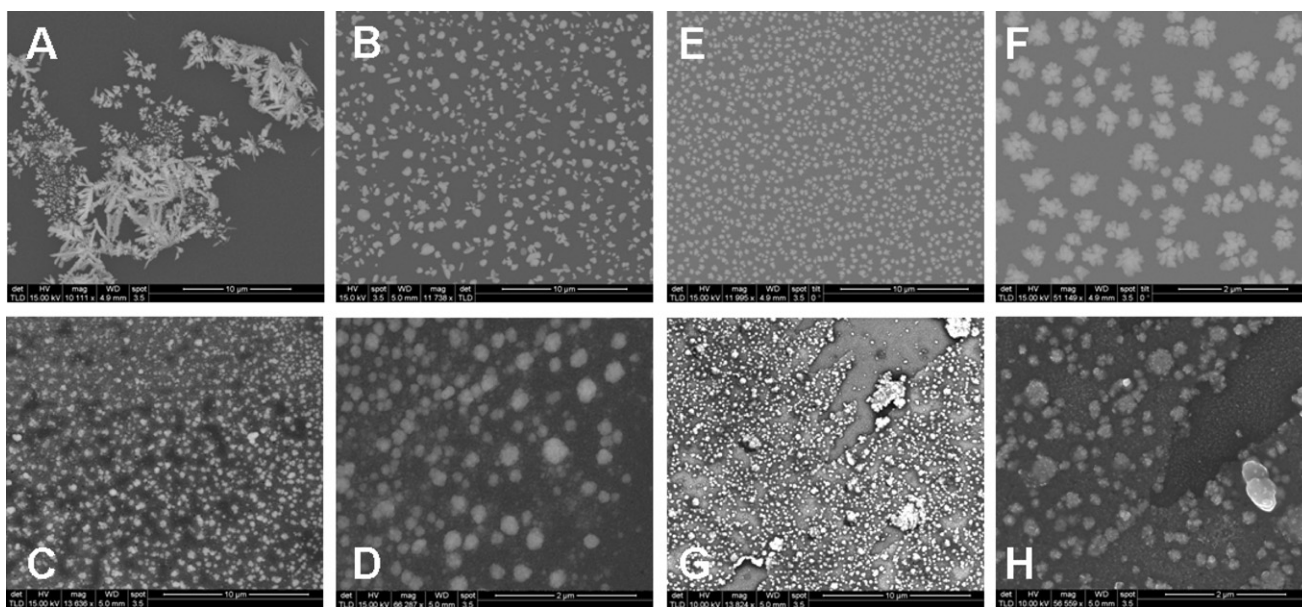


Fig. 7. SEM images of Ag deposits on GC electrode from (a) deposition at -0.15 V vs $\text{Ag}/\text{AgCl}/\text{KCl}$ from 5 mM AgNO_3 in 0.1 M KNO_3 ; (b) deposition at 0.20 V vs $\text{Ag}/\text{AgCl}/\text{KCl}$ from 5 mM AgNO_3 in 0.1 M KNO_3 ; (c) deposition at -0.80 V vs Ag QRE from 20 mM AgBF_4 in $[\text{BMIm}][\text{BF}_4]$; (d) higher magnification of sample from (c); (e) deposition at -0.75 V vs $\text{Ag}/\text{AgOTf}/[\text{C}_4\text{mPyr}][\text{TFSI}]$ from 10 mM AgOTf in dry $[\text{C}_4\text{mPyr}][\text{TFSI}]$; (f) higher magnification of sample from (e); (g) deposition at -0.80 V vs $\text{Ag}/\text{AgOTf}/[\text{C}_4\text{mPyr}][\text{TFSI}]$ from 10 mM AgOTf in wet $[\text{C}_4\text{mPyr}][\text{TFSI}]$; (h) higher magnification of sample from (g).

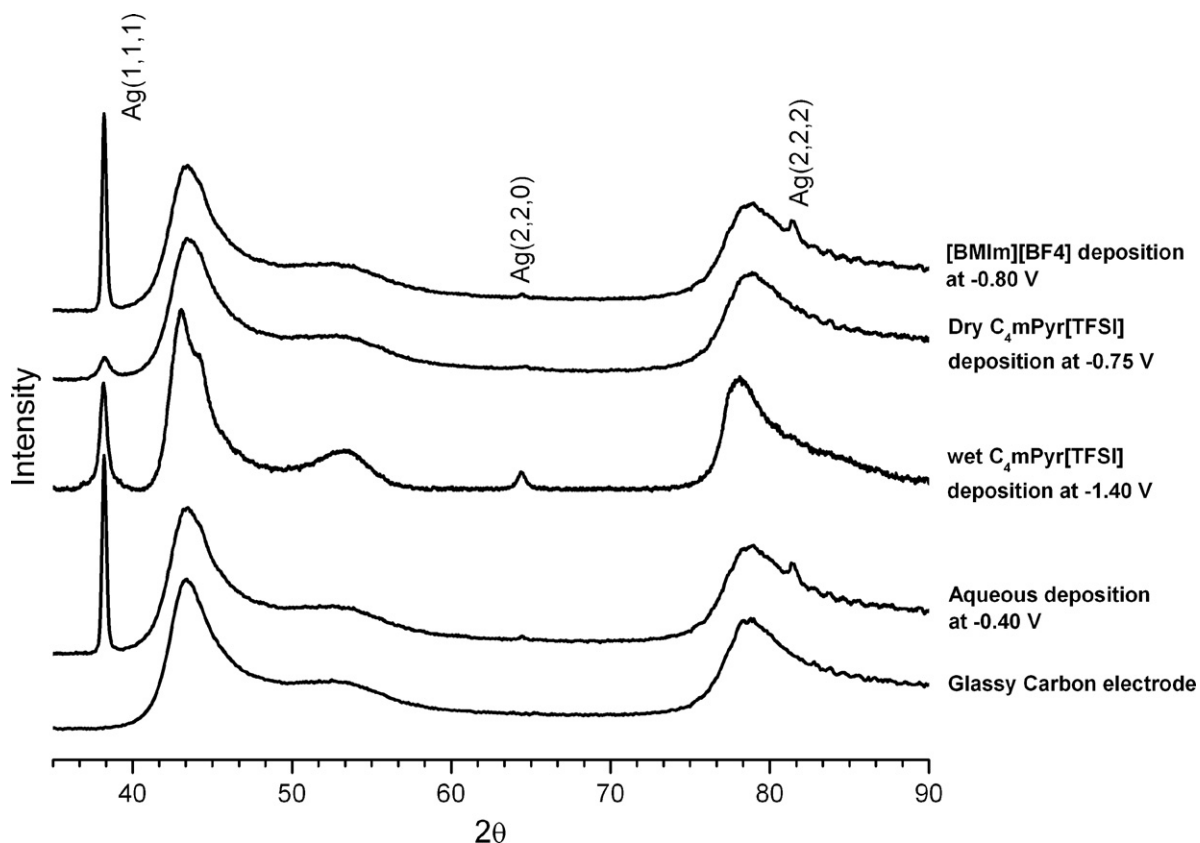


Fig. 8. X-ray diffraction patterns for Ag deposits on GC electrodes from [BMIm][BF₄], wet and dry [C₄mPyr][TFSI] and AgNO₃ in 0.1 M KNO₃. Data collected using a General Area Detector Diffraction System (GADDS).

atmospheric uptake of water. Thus the increase in available Ag⁺ ions at the electrode surface, in combination with the required high overpotentials for deposition due to the change in IL properties, results in greater numbers of Ag nuclei forming on the GC electrode. The obvious assumption here is that the water impurity does not interact with the Ag⁺ ions in solution to change its speciation; however, the data presented in this study does not conclusively identify this relationship. Regardless of the nature of the water interaction, it is suggested that control of water impurity in this IL can allow experimental control over the type of morphology obtained upon deposition. Unfortunately, the data obtained for the [BMIm][BF₄] did not show any evidence for progressive nucleation, thus it is difficult to know if the trends observed for wet and dry [C₄mPyr][TFSI] are indicative of IL behaviour in general or if this is unique to [C₄mPyr][TFSI].

3.3. SEM and XRD characterisation of electrodeposits

Scanning electron microscopy (SEM) images were recorded to characterise the silver electrodeposits formed from both IL systems and 0.10 M KNO₃/water after the electrochemical measurements. To allow for meaningful comparisons between all the systems studied, the charge passed during the electrodeposition process was kept constant (90 mC cm⁻²). In the case of the aqueous system, since the chronoamperometry data suggested a change in mechanism as a function of reduction potential, two deposition potentials were chosen to encompass both regions to further probe the impact of the electrodeposition mechanism on the deposition morphology.

Fig. 7 shows typical SEM images of silver (confirmed by EDX analysis) electrodeposited from [BMIm][BF₄], [C₄mPyr][TFSI] and 0.10 M KNO₃/water. Fig. 7a shows an SEM image of deposits

from the 0.10 M KNO₃/water system obtained from a deposition potential of -0.15 V and 90 mC cm⁻². The morphology of the deposited silver shows significant dendritic growth and a fern like structure. This deposition morphology implies that the CA data, which suggested at a potential of -0.15 V the Ag nucleation and growth mechanism is progressive in nature during the initial stages of deposition. However, if the deposition potential is changed to +0.20 V, as shown in Fig. 7b, the deposits show a reasonably regular size distribution in agreement with an instantaneous nucleation-growth mechanism as determined by chronoamperometric studies.

In the case of [BMIm][BF₄] (Fig. 7c), it can be seen that a fairly uniform particle size distribution is observed on the GC electrode surface. The silver deposits in spherical particulates of which there is an underlying layer of spheres of 100–300 nm in diameter, upon which larger deposits have grown due to the high overpotential applied (Fig. 7d). Again this behaviour is complimentary to the CA data which suggests that the mechanism is instantaneous nucleation and growth in nature.

Because the silver deposition mechanism is strongly related to the water content of the [C₄mPyr][TFSI], SEM images were recorded for both the dry and wet cases. In the dry [C₄mPyr][TFSI] SEM images (Fig. 7e and f) show that the deposited particle size does not vary substantially, which is in agreement with an instantaneous nucleation-growth mechanism. The anisotropic nature of the particles formed is interesting and suggests that the IL may be acting as a growth directional agent, as seen for many organic surfactants [35,36] and inorganic salts [37] that have been employed as additives in electroplating metals. Generally these additives bind preferentially to certain crystal facets that inhibit or promote growth in particular directions, which may also be the case in the present study.

If the silver deposition is carried out in [C₄mPyr][TFSI] that has been allowed to absorb atmospheric H₂O, the SEM images (Fig. 7g and h) show significant differences to the dry case. The SEM images show a random distribution of spherical particles from sub micron sized upwards. All of the larger structures are layered on top of an underlying layer of sub-micron sized spherical particles similar to the case of [BMIm][BF₄]. The particle size distribution behaviour is consistent with the proposed change in mechanism from instantaneous to progressive nucleation and growth as suggested by the CA data. The effect of water in this system can clearly have a significant effect on the deposition morphologies.

XRD studies were carried out to investigate if the morphology of the electrodeposits was related to any preferred crystallographic orientation of the silver particles. For silver electrodeposited from [BMIm][BF₄] at a potential of –0.80 V characteristic peaks at $2\theta = 38.2^\circ$, 64.5° and 81.4° are observed due to the {1 1 1}, {2 2 0} and {2 2 2} crystal planes of polycrystalline silver, respectively, with a marked increase in intensity of the {1 1 1} plane compared to the other planes (Fig. 8). The underlying GC substrate provides its own XRD pattern which is indicated in Fig. 8. In the case of silver electrodeposited from aqueous solution a similar XRD pattern was obtained with an intense {1 1 1} reflection. In contrast, in the case of dry [C₄mPyr][TFSI] the {1 1 1} peak is less intense when compared to the {2 2 0} crystal plane. However, when atmospheric water was present in [C₄mPyr][TFSI] a significant increase in intensity of the {1 1 1} crystal plane in particular is observed that is similar to the XRD pattern obtained for the silver electrodeposit from aqueous solution. This further indicates the role that adventitious water plays in influencing the morphology and crystallography of the silver electrodeposit.

4. Conclusions

The electrodeposition of silver onto glassy carbon electrodes was investigated in aqueous media and two different ionic liquids, [C₄mPyr][TFSI] and [BMIm][BF₄]. The voltammetric data obtained shows for all three systems that electrodeposition of Ag proceeds via a nucleation and growth type mechanism. In the case of the aqueous system, the data shows that the removal of silver from the glassy carbon electrode after plating is not chemically reversible and trace silver always remains, presumably due to the formation of silver oxide. However, in the case of the ILs, close to full reversibility is observed and no additional reactions of the deposited silver are observed. The voltammetry for [C₄mPyr][TFSI] is further complicated when water from atmospheric absorption is present. Under these conditions a significant shift in E_p^{red} and E_p^{ox} is observed; this effect is attributed to silver nanoparticle formation from the reaction of dissolved Ag⁺ ions with water. The formation of nanoparticles has been confirmed by UV/vis spectroscopy, EDX analysis and TEM images. In the case of the ILs, it was found that the electrodeposition mechanism proceeded through an instantaneous nucleation–growth mechanism as deduced by analysis of chronoamperometry data and confirmed by SEM imaging. Significantly, for the case of [C₄mPyr][TFSI], it was demonstrated

that the uptake of atmospheric water in the IL resulted in a change in the electrodeposition mechanism to progressive nucleation and growth. This is in agreement with studies carried out in aqueous solution that also demonstrated the same electrodeposition mechanism. Interestingly, continuous exposure of the silver salt/IL solution to atmospheric conditions resulted in the extensive formation of silver nanoparticles that interfere with electrodeposition experiments by adhering to the glassy carbon electrode. Overall it has been demonstrated from these studies that the water content of ionic liquids can significantly influence metal electrodeposition processes and under controlled conditions may offer a route to tuning the morphology of the resulting deposits.

References

- [1] F. Endres, D. MacFarlane, A. Abbott, *Electrodeposition from Ionic Liquids*, Wiley-VCH, Weinheim, 2008.
- [2] W. Simka, D. Puszczczyk, G. Nawrat, *Electrochim. Acta* 54 (2009) 5307.
- [3] R. Bomparola, S. Caporali, A. Lavacchi, U. Bardi, *Surf. Coat. Technol.* 201 (2007) 9485.
- [4] S. Zein El Abedin, F. Endres, *Electrochim. Acta* 54 (2009) 5673.
- [5] G. Martínez-Castañón, N. Niño-Martínez, F. Martínez-Gutiérrez, J. Martínez-Mendoza, F. Ruiz, *J. Nanopart. Res.* 10 (2008) 1343.
- [6] C.-N. Lok, C.-M. Ho, R. Chen, Q.-Y. He, W.-Y. Yu, H. Sun, P.K.-H. Tam, J.-F. Chiu, C.-M. Che, *J. Biol. Inorg. Chem.* 12 (2007) 527.
- [7] C.A. Zell, F. Endres, W. Freyland, *Phys. Chem. Chem. Phys.* 1 (1999) 697.
- [8] F. Endres, W. Freyland, *J. Phys. Chem. B* 102 (1998) 10229.
- [9] X.H. Xu, C.L. Hussey, *J. Electrochem. Soc.* 139 (1992) 1295.
- [10] F. Endres, W. Freyland, B. Gilbert, *Ber. Bunsen-Ges.* 101 (1997) 1075.
- [11] P. He, H. Liu, Z. Li, Y. Liu, X. Xu, J. Li, *Langmuir* 20 (2004) 10260.
- [12] C. Fu, H. Zhou, W. Peng, J. Chen, Y. Kuang, *Electrochem. Commun.* 10 (2008) 806.
- [13] K. Yasushi, D. Satomi, M. Takashi, K. Tomiya, *J. Electrochem. Soc.* 148 (2001) C102.
- [14] S. Arimoto, H. Kageyama, T. Torimoto, S. Kuwabata, *Electrochem. Commun.* 10 (2008) 1901.
- [15] M.-C. Tsai, D.-X. Zhuang, P.-Y. Chen, *Electrochim. Acta* 55 (2010) 1019.
- [16] A.I. Bhatt, A.M. Bond, *J. Electroanal. Chem.* 619 (2008) 1.
- [17] M.G. Freire, C.M.S.S. Neves, I.M. Marrucho, J.A.P. Coutinho, A.M. Fernandes, *J. Phys. Chem. A* 114 (2010) 3744.
- [18] G.A. Snook, A.S. Best, A.G. Pandolfo, A.F. Hollenkamp, *Electrochem. Commun.* 1405 (2006) 8.
- [19] D.J. Schiffrin, *J. Electroanal. Chem.* 199 (1986) 201.
- [20] A.R. Harris, A.K. Neufeld, A.P. O'Mullane, A.M. Bond, R.J.S. Morrison, *J. Electrochem. Soc.* 152 (2005) C577.
- [21] W. Obretenov, T. Kossev, V. Bostanov, E. Budevski, *J. Electroanal. Chem.* 159 (1983) 257.
- [22] V. Bansal, V. Li, A.P. O'Mullane, S.K. Bhargava, *CrystEngComm* 12 (2010) 4280.
- [23] A.I. Bhatt, A. Mechler, L.L. Martin, A.M. Bond, *J. Mater. Chem.* 2241 (2007) 17.
- [24] I. Pastoriza-Santos, L.M. Liz-Marzan, *Langmuir* 2888 (2002) 18.
- [25] A. O'Mahony, D.S. Livestier, L. Aldous, C. Hardacre, R.G. Compton, *J. Chem. Eng. Data* 2884 (2008) 53.
- [26] M.O. Kestner, A.L. Allred, *J. Am. Chem. Soc.* 94 (1972) 7189.
- [27] M. Pazicky, F. Rominger, M. Limbach, *Acta Cryst. E* 66 (2010) m724.
- [28] D. Sroczynski, A. Grzejdzia, *J. Incl. Phenom. Macrocyclic Chem.* 42 (2002) 99.
- [29] B. Scharifker, G. Hills, *Electrochim. Acta* 879 (1983) 28.
- [30] A.I. Bhatt, A.M. Bond, J. Zhang, *J. Solid State Electrochem.* 1593 (2007) 11.
- [31] C.L. Hussey, X. Xu, *J. Electrochem. Soc.* 1886 (1991) 138.
- [32] A. Milchev, E. Vassileva, V. Kertov, *J. Electroanal. Chem.* 107 (1980) 323.
- [33] Y. Cao, A.C. Wert, *J. Electrochem. Soc.* 149 (2002) C223.
- [34] G.A. Gunawardena, G.J. Hills, I. Montenegro, *Electrochim. Acta* 693 (1978) 23.
- [35] M.S. El-Deab, T. Sotomura, T. Ohsaka, *Electrochim. Acta* 52 (2006) 1792.
- [36] D. Romanska, M. Mazur, *Langmuir* 19 (2003) 4532.
- [37] B. Plowman, S.J. Ippolito, V. Bansal, Y.M. Sabri, A.P. O'Mullane, S.K. Bhargava, *Chem. Commun.* (2009) 5039.